PERGAMON

International Journal of Heat and Mass Transfer 43 (2000) 2917–2930

International Journal of HEAT and MASS TRANSFER

www.elsevier.com/locate/ijhmt

An analytical model for transport from quasi-steady and periodic accelerations on spacecraft

Robert J. Naumann

Materials Science, University of Alabama in Huntsville, Huntsville, AL 35899, USA

Received 23 March 1999; received in revised form 9 October 1999

Abstract

A simplified analytical model of the coupled flow, heat, and mass transfer in the core region of a rectangular, low aspect ratio flow channel has been developed that can predict the magnitude of the flows and the convective transport resulting from small transverse steady and periodic accelerations typically associated with manned spacecraft. The effects of stabilizing and destabilizing axial gradients are determined for both steady and time dependent transverse accelerations. It is found that the time average of the heat and mass transport scales as the square of the Grashof number and is inversely proportional to the 7/2 power of the frequency. Furthermore, it is shown that the effects of multi-frequency disturbances are additive making it possible to integrate over a properly weighted power spectral density spectrum in order to obtain the net flow and transport. The relative transport from steady and periodic accelerations was estimated for the types of experiments germane to this model that are typically carried out in microgravity. It was also found that a stabilizing axial gradient has little effect on the flows and transport at higher frequencies, suggesting the possibility of testing the g-jitter predictions on the ground. Finally it is shown that the start-up transients can have profoundly different effects depending on the phase of the acceleration at the starting time.

1. Introduction

The acceleration environment on a large spacecraft such as the Shuttle or the International Space Station may be characterized by a low-level, quasi-steady acceleration from drag and gravity gradient effects, which ranges from 1 to 10 μg, and a spectrum of larger amplitude, periodic accelerations with frequencies ranging from sub hertz to tens of hertz (sometimes referred to as "g-jitter"). The latter are associated with the natural frequencies of the various bending modes of the structure and are excited by crew motion, onboard reciprocating machinery, and by impulsive transients such as thruster firings.

There have been numerous attempts to model the effects of these accelerations for a generic class of experiments, usually some form of Bridgman-type crystal growth. Examples of these efforts are given in Refs. [1–7]. Unfortunately, there are virtually no definitive experimental data with which to compare these model predictions. While it is possible to model experiments numerically in great detail using realistic configurations, it is difficult to obtain a general theory from such computations or to derive scaling laws that would allow optimizing the design of a particular experiment or the extrapolation to a different set of experiment conditions. Also, tracking higher frequency accelerations numerically until a

E-mail address: naumannr@email.uah.edu (R.J. Naumann).

0017-9310/00/$ - see front matter
PII: S0017-9310(99)00340-3

Nomenclature

a	half-height $= h/2$
A	aspect ratio $= h/L$
C	concentration
D	solutal diffusivity
f	applied vibrational frequency
g	acceleration
Gr	Grashof number $= g_y(\beta\nabla T + \gamma\nabla C)a^4/\nu^2$
h	height of the flow chamber
L	length of the flow chamber
Nu	Nusselt number = convective thermal transport/conductive thermal transport
p	pressure
Pr	Prandtl number $= \nu/\kappa$,
Ra_x^T	thermal Rayleigh number $= g_x\beta\nabla T a^4/\nu\kappa$
Ra_x^S	solutal Rayleigh number $= g_x\gamma\nabla C a^4/\nu D$
Sc	Schmidt number $= \nu/D$
Sh	Sherwood number = convective solutal transport/diffusive solutal transport
T	temperature
u	x-component of velocity
v	y-component of velocity the coefficient of thermal expansion
x	position along L
y	position along h
U	dimensionless velocity $= ua/\nu$

Greek symbols

β	coefficient of thermal expansion
γ	coefficient of solutal expansion
η	dimensionless coordinate $= y/a$
Θ	dimensionless temperature perturbation $= \breve{T}/(a\nabla T)$
κ	thermal diffusivity
μ	absolute viscosity
ν	kinematic viscosity $= \mu/\rho$
ρ	density
τ	momentum relaxation time $= a^2/\nu$
χ	dimensionless compositional perturbation $= \breve{C}/(a\nabla C)$
ω	angular frequency $= 2\pi f$
Ω	dimensionless frequency $= \omega a^2/\nu$

Superscripts

$'$	differentiation with respect to η
$\tilde{}$	complex quantity
$\hat{}$	real amplitude
$\breve{}$	perturbation solution

Subscripts

x and y	components of acceleration

steady solution is reached can consume a significant amount of computer time. An analytical model, even though it must be simplified to remain tractable, overcomes these difficulties and can provide considerable insight and useful scaling laws.

The model presented here considers only the core flow in a low aspect ratio (length $\gg$ height) rectangular channel with a uniform density gradient, which represents a simplified Bridgman configuration as illustrated schematically in Fig. 1. This simplification eliminates the analytical difficulties in describing the two-dimensional turning flows near the ends and focuses instead on the one-dimensional flow near the midpoint of the flow channel for which closed form analytical solutions can be obtained. Of primary interest will be the heat (or mass) transport across the midplane of the flow cell, which must also appear at the ends. Thus, it should be possible to predict how the acceleration environment affects the thermal and solutal transport to the growth interface from the simple one-dimensional flow model.

The steady flow and heat transfer in a shallow horizontal cavity with differentially heated end walls was treated by Cormack, Leal, and Imberger [8]. They expanded the Navier–Stokes equations in terms of the aspect ratio A, defined as the ratio of height h to length L of the cavity, and showed that, in the limit of small A and small Rayleigh numbers, the flow in the core region was parallel to the walls with the warmer fluid flowing from hot to cold in the upper half of the

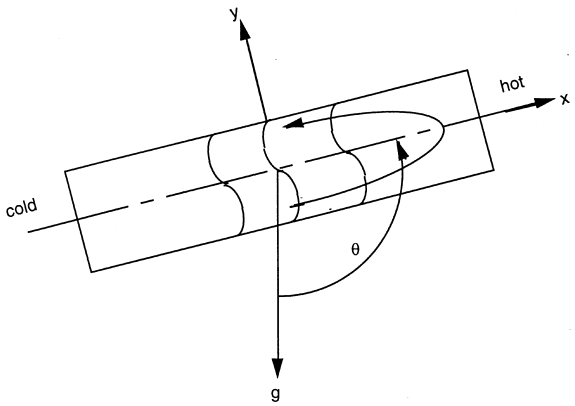

Fig. 1. Schematic of the geometry used in the model. The thermal gradient is positive along the x-axis so for $\theta = 0$, the Ra_x is positive and the system is in the unstable (cold over hot) thermal configuration. The curved lines represent isotherms distorted by the flow.

cavity above a counter flow of the cooler fluid in the lower half of the cavity. The temperature gradients are constant but displaced along the streamlines. A solution was found by matching the core flow to the first several terms of an asymptotic expansion of the flow in the end region. This solution was compared to numerical solutions [9] as well as to experimental measurements [10]. It was found that the assumption of parallel core flow was valid provided $A \leq 0.25$ and that their solution was found to be in excellent agreement with numerical as well as experimental results provided the Rayleigh number satisfied $Ra^2A^3 \leq 10^5$ which, for small A, carries the theory well into the regime in which heat transfer is dominated by convection. For larger values of the Rayleigh number, the required product of Ra^2A^3 to provide the same convective transport, which is characterized by the Nusselt number, increases rapidly; eventually approaching the case in which the Nusselt number becomes independent of A and $\sim Ra^{1/4}$ as predicted from boundary layer theory [11].

The Gr in this paper is defined in terms of the density gradient and the half-width of the chamber, which is different from the more conventional definition used by Cormack et al. Since the Gr here is equivalent to $A/256$ times Cormack's definition, the range of validity in the present notation is $Gr^2Pr^2A \leq 10^5/256 \approx 400$.

2. Derivation of the governing equations

An alternative approach to that taken by Cormack et al. is to derive time-dependent equations of motion in the core region directly using the assumptions of parallel laminar flow and constant thermal (or solutal) gradients in the core region. If the vertical component of velocity vanishes, the continuity equation requires that the horizontal velocity u be a function of y only and the advective momentum terms also vanish. In the Boussinesq approximation, the x and y momentum equations reduce to

$$\frac{\partial u(y,t)}{\partial t} = -\frac{1}{\rho_0}\frac{\partial p}{\partial x} + \nu\frac{\partial^2 u(y,t)}{\partial y^2} + \left[1-\beta(T-T_0)\right]g_x \tag{1}$$

and

$$0 = -\frac{1}{\rho_0}\frac{\partial p}{\partial y} + \left[1-\beta(T-T_0)\right]g_y. \tag{2}$$

The pressure terms are eliminated by cross differentiating the above and subtracting to give

$$\frac{\partial^2 u(y,t)}{\partial t \partial y} = \nu\frac{\partial^3 u(y,t)}{\partial y^3} - \beta\frac{\partial T}{\partial y}g_x + \beta\frac{\partial T}{\partial x}g_y. \tag{3}$$

Assume $T(x,y,t)$ can be written as $T_0 + x\Delta T/L + \breve{T}(y,t)$ where $T = T_0 + \Delta T x/L$ is the base state and $\breve{T}(y,t)$ is a perturbation on the temperature field. Since $\nu = 0$, $u \cdot \nabla T = u(y)\Delta T/L$ and any change in T will be a function of y only.

Now a partial integration of Eq. (3) over y is carried out. This introduces a constant and an arbitrary function $F(x)$. However, the continuity equation tells us that the core flow u is a function of y only; therefore, we set $F(x) = 0$. If we take $y = 0$ as the center line of cavity, the "no-net flow condition" requires that u and $\partial u/\partial t$ have terms of odd powers of y only, which requires the constant be set to zero. Thus, the governing equations for flow and heat transport for laminar core flow in a two-dimensional horizontal cavity may be written as

$$\frac{\partial u(y,t)}{\partial t} = \nu\frac{\partial^2 u(y,t)}{\partial y^2} + g_y\beta\frac{\Delta T}{L}y - g_x\beta\breve{T}(y,t) \tag{4}$$

$$\frac{\partial \breve{T}(y,t)}{\partial t} + u(y,t)\Delta T/L = \kappa\frac{\partial^2 \breve{T}(y,t)}{\partial y^2}. \tag{5}$$

This derivation can be generalized to include solute transport by employing the same arguments to the solute transport equation, which gives

$$\frac{\partial \breve{C}(y,t)}{\partial t} + u(y,t)\Delta C/L = D\frac{\partial^2 \breve{C}(y,t)}{\partial y^2} \tag{6}$$

where $C(x,\ y,\ t) = x\Delta C/L + \breve{C}(y,\ t)$. The effect of the solutal gradient must be added to the momentum equation to give

$$\frac{\partial u(y,t)}{\partial t} = \nu\frac{\partial^2 u(y,t)}{\partial y^2} + g_y(\beta\nabla T + \gamma\nabla C)y - g_x\left(\beta\breve{T}(y,t) + \gamma\breve{C}(y,t)\right). \tag{7}$$

To simplify these equations, introduce a dimensionless length $\eta = y/a$, a dimensionless temperature Θ and a dimensionless concentration χ defined as

$$\Theta(\eta,t) = \frac{\breve{T}(\eta,t)}{a\nabla T} \tag{8}$$

and

$$\chi(\nu,t) = \frac{\breve{C}(\eta,t)}{a\nabla C}. \tag{9}$$

The momentum equation may be written in terms of a dimensionless velocity (or Reynolds number) $U(\eta,t) = u(\eta,t)a/\nu$ as

$$\dot{U}\tau = U'' + Gr_y\eta - Ra_x^{\mathrm{T}}\Theta/Pr - Ra_x^{\mathrm{S}}\chi/Sc \tag{10}$$

The subscripts x and y refer to the components of the g vector. The transport equations then become

$$\dot{\theta}\tau Pr + UPr = \Theta'' \tag{11}$$

and

$$\dot{\chi}\tau Sc + USc = \chi''. \tag{12}$$

The boundary conditions are $u(\pm 1) = 0$ (no slip at the walls), $\int_{-1}^{1} u(\eta)\,\mathrm{d}\eta = 0$ (conservation of flow), $\breve{C}'(\pm 1) = 0$ (no solute transmitted through the walls), and either $\breve{T}(\pm 1) = 0$ (conducting walls), or $T'(\pm 1) = 0$ (adiabatic walls) where the prime denotes differentiation with respect to η.

Usually, the Nusselt number is defined as the ratio of total heat transport to diffusive (conductive) heat transport. Since we will mostly be dealing with small convective transport, it is more convenient to define a modified Nusselt number as the ratio of convective transport across a boundary to conducted transport. Integrating the convective heat flow through a plane normal to the x-axis and dividing this by the diffusive transport, we obtain,

$$Nu(t) = \frac{\int_{-1}^{1} u(t,\eta)\rho C_v T(t,\eta)\,\mathrm{d}\eta}{-\int_{-1}^{1} K\nabla T\,\mathrm{d}\eta} = -\frac{Pr}{2}\int_{-1}^{1} U(t,\eta)\Theta(t,\eta)\,\mathrm{d}\nu. \tag{13}$$

Similarly, a modified Sherwood number is defined as the ratio of solute transported by convection to that by diffusion.

$$Sh(t) = \frac{\int_{-1}^{1} u(t,\eta)C(t,\eta)\,\mathrm{d}\eta}{-2D\nabla C} = -\frac{Sc}{2}\int_{-1}^{1} U(t,\eta)\chi(t,\eta)\,\mathrm{d}\nu. \tag{14}$$

3. Cases for which closed form solutions exist

Case 1 (g_x and g_y constant)**.** This case was considered in Ref. [12] for adiabatic walls in which the flows were driven either by thermal gradients or by solutal gradients. A more general solution for flows driven by any combination of thermal and/or solutal gradients can be written as

$$U(\eta) = \frac{Gr_y}{b^3}\left[\frac{-\sin(b)\sinh(b\eta) + \sinh(b)\sin(b\eta)}{\cos(b)\sinh(b) + \sin(b)\cosh(b)}\right] \tag{15}$$

$$\Theta(\eta) = -\frac{Gr_y Pr}{b^5}\left[\frac{\sin(b)\sinh(b\eta) + \sinh(b)\sin(b\eta)}{\cos(b)\sinh(b) + \sin(b)\cosh(b)} - b\eta\right] \tag{16}$$

$$\chi(\eta) = -\frac{Gr_y Sc}{b^5}\left[\frac{\sin(b)\sinh(b\eta) + \sinh(b)\sin(b\eta)}{\cos(b)\sinh(b) + \sin(b)\cosh(b)} - b\eta\right] \tag{17}$$

where $b = [Ra_x^{\mathrm{T}} + Ra_x^{\mathrm{S}}]^{1/4}$. In this notation, a positive Rayleigh number denotes the destabilizing configuration. There is a singularity in the denominator at $b = 2.365$ which corresponds to a combined Rayleigh number (thermal + solutal) of 31.284. In terms of the more conventional definition of the thermal Rayleigh number when dealing with unstable convection, $Ra = g\beta\Delta TL^3/\nu\kappa$, the singularity in Eqs. (15)–(17) indicates a critical Rayleigh number of $Ra = 500.5/A^4$, where A is the aspect ratio.

For the stabilizing configuration, b will be complex. The denominator in Eqs. (15)–(17) becomes $-8\sqrt{2}Gr_x^3[\sin(b^*)\cos(b^*) + \sinh(b^*)\cosh(b^*)]$ where $b^* = \sqrt{2}|Ra_x^{\mathrm{T}} + Ra_x^{\mathrm{S}}|$, and the singularity is removed.

As b vanishes (pure transverse acceleration), the above equations reduce to simple polynomials,

$$U(\eta) = -\frac{Gr_y}{6}\left(\eta^3 - \eta\right) + O(b^2) \tag{18}$$

$$\Theta(\eta) = -\frac{Gr_y Pr}{360}\left(3\eta^5 - 10\eta^3 + 15\eta\right) + O(b^2) \tag{19}$$

$$Nu = -\frac{Pr}{2}\int_{-1}^{1} U(\eta)\Theta(\eta)\,\mathrm{d}\eta = \frac{2}{2835}Gr_y^2 Pr^2 \tag{20}$$

For thermally conductive walls, the solutions becomes

$$U(\eta) = \frac{Gr_y}{2b^2}\left[\frac{-\sin(b)\sinh(b\eta) + \sinh(b)\sin(b\eta)}{\sin(b)\sinh(b)}\right] \tag{21}$$

$$\Theta(\eta) = -\frac{Gr_y Pr}{2b^4}\left[\frac{\sin(b)\sinh(b\eta) + \sinh(b)\sin(b\eta)}{\sin(b)\sinh(b)} - 2b\eta\right] \tag{22}$$

Here the first singularity occurs at $b = \pi$, which corresponds to a combined Rayleigh number of $\pi^4 = 97.406$ as defined in this paper, or to the more conventional $Ra = 1559/A^4$. This is in exact agreement with the critical Rayleigh number found in the stability analysis of this configuration by Gershuni and Lyubimov [6].

For the stabilizing configuration, b will be complex, the denominator in Eqs. (15)–(17) becomes $-4Gr_x^2[\sin^2(b^*)\cosh^2(b^*) + \sinh^2(b^*)\cos^2(b^*)]$ where

$b^* = \sqrt{2}|Ra_x^T + Ra_x^S|$, and the singularity is again removed.

As b vanishes, Eq. (21) reduces to Eqs. (18) and (22) and Nu become

$$\Theta(\eta) = -\frac{Gr_y Pr}{360}\left(3\eta^5 - 10\eta^3 + 7\eta\right) + O(b^2) \tag{23}$$

$$Nu = -\frac{Pr}{2}\int_{-1}^{1} U(\eta)\Theta(\eta)\,\mathrm{d}\eta = \frac{1}{4725}Gr_y^2 Pr^2 \tag{24}$$

These equations describing the flow and transport in a narrow horizontal cavity for $Ra_x = 0$ are identical to those obtained by Cormack, Leal, and Imberger [7]. Bejan and Tien [13] also obtained a solution for the flow in a long horizontal cylindrical pipe with differentially heated ends. Their results were similar to Eq. (18) except the 6 in the denominator was replaced by an 8, indicating that the flows predicted for two-dimensional cavities can be reasonably expected to apply to three-dimensional cylindrical geometries with a minor correction to account for the additional viscous drag force from the walls.

Case 2 (Periodic transverse acceleration, constant axial acceleration)**.** For $g(t) = Re[\tilde{g}e^{i\omega t}] = \hat{g}\cos(\omega t)$, assuming u and T are zero at $t = 0$, the solution to Eqs. (10) and (11) may be written,

$$U(\eta, t) = -\hat{G}r_y \sum_n \frac{2\cos(n\pi)\sin(n\pi\eta)}{n\pi \mathrm{Den}_n} \times \left[A_n\cos(\omega t) + B_n\sin(\omega t) - A_n e^{-n^2\pi^2 t/\tau}\right] \tag{25}$$

For conducting walls,

$$\Theta(\eta, t) = \hat{G}r_y Pr \sum_n \frac{2\cos(n\pi)\sin(n\pi\eta)}{n\pi \mathrm{Den}_n}\left[C_n\cos(\omega t) + D_n\sin(\omega t) + \frac{A_n e^{-n^2\pi^2 t/\tau}}{n^2\pi^2(1+Pr)} - \left(C_n + \frac{A_n}{n^2\pi^2(1+Pr)}\right)e^{-n^2\pi^2 t/Pr\tau}\right] \tag{26}$$

where

$$A_n = n^2\pi^2\left(n^4\pi^4 + \Omega^2 Pr^2 - Ra_x\right)$$

$$B_n = \Omega\left(n^4\pi^4 + \Omega^2 Pr^2 + PrRa_x\right)$$

$$C_n = \left(n^4\pi^4 - \Omega^2 Pr - Ra_x\right)$$

$$D_n = n^2\pi^2\Omega(1+Pr)$$

$$\mathrm{Den}_n = Ra_x^2 - 2(n^4\pi^4 - \Omega^2 Pr)Ra_x + \left(n^4\pi^4 + \Omega^2\right)\left(n^4\pi^4 + \Omega^2 Pr^2\right)$$

To obtain the Nusselt number, the series product may be integrated over η by making use of the orthogonal properties of $\sin(n\pi\eta)$. After the transients die out, the resulting expression may be broken into a periodic term whose amplitude is

$$\hat{N}u = \hat{G}r_y^2 Pr^2 \sum_n \frac{(A_n D_n + B_n C_n)}{n^2\pi^2 \mathrm{Den}_n^2} \tag{27}$$

and a steady term

$$\langle Nu\rangle = \hat{G}r_y^2 Pr^2 \sum_n \frac{(A_n C_n + B_n D_n)}{n^2\pi^2 \mathrm{Den}_n^2}$$

which reduces to

$$\langle Nu\rangle = \hat{G}r_y^2 Pr^2 \sum_n \frac{1}{Ra_x^2 - 2(n^4\pi^4 - \Omega^2 Pr)Ra_x + \left(n^4\pi^4 + \Omega^2\right)\left(n^4\pi^4 + \Omega^2 Pr^2\right)} \tag{29}$$

Here one can see the effect of the stabilizing gradient ($Ra_x < 0$) on the resulting flows and transport. For $Ra_x = 0$, this expression further reduces to

$$\langle Nu\rangle = \hat{G}r_y^2 Pr^2 \sum_n \frac{1}{\left(n^4\pi^4 + \Omega^2\right)\left(n^4\pi^4 + \Omega^2 Pr^2\right)}. \tag{30}$$

These series converge for all values of Ω and Pr as can be demonstrated by the integral test. In the limit $\Omega \to 0$, the series for $\langle Nu\rangle$ converges rapidly to 1/9450, which is exactly half the result from the steady state case. This difference is due to the latter taking the time average over the square of a periodic acceleration, which yields the mean square value of 1/2.

For large Ω, the sum over n may be replaced by an integral giving the result

$$\langle Nu\rangle \approx \frac{\hat{G}r_y^2}{\Omega^{7/2}}\frac{Pr^{1/2}(Pr^{3/2} - 1)}{2^{3/2}(Pr^2 - 1)}; \quad \Omega \gg 1. \tag{31}$$

Note that for large Ω and large Pr, $Nu \sim \hat{G}r_y^2\Omega^{-7/2}$. This inverse 7/2 power dependence was also found by Perra in his numerical analysis of periodic acceleration on diffusion [7].

For the case of adiabatic walls, the boundary condition requires an additional term in the solution of Eq. (11), i.e.,

$$\Theta(\eta, t) = \hat{G}r_y Pr\ Re\left[\sum_n \tilde{B}_n\left(\sin(n\pi\eta) - \frac{n\pi\cos(n\pi)\sinh\left(\sqrt{i\Omega\ Pr}\,\eta\right)}{\sqrt{i\Omega\ Pr}\cosh\left(\sqrt{i\Omega\ Pr}\right)}\right)e^{i\omega t}\right] \tag{32}$$

where

$$\tilde{B}_n = \frac{2\cos(n\pi)}{(n^2\pi^2 + i\Omega)(n^2\pi^2 + i\Omega\ Pr)}.$$

This complex form of the solution is equivalent to Eq. (26) except for the second term in the bracket. With this additional term, there is no convenient way to integrate the series product as before. Therefore, it is necessary to evaluate the *Nu* by integrating Eq. (13) numerically. Note, however, that this term diminishes with increasing $\Omega\ Pr$. Therefore, for higher frequencies, the solution for conductive walls may be used for either case

Case 3 (Transverse acceleration contains multiple frequencies, no axial acceleration)**.** For this case, let $g_x = 0$ and $\tilde{g}_y(t) = \sum_j \tilde{g}_j e^{i\omega_j t}$. Since the governing equations are linear, their solutions are sums of the contributions of the individual frequencies and may be written in the form,

$$\tilde{U}(\eta, t) = \sum_j \tilde{G}r_j \sum_n \left[a_{nj}\cos(\omega_j t) + b_{nj}\sin(\omega_j t)\right]\sin(n\pi\eta) \tag{33}$$

$$\tilde{\Theta}(\eta, t) = Pr\sum_k \tilde{G}_k \sum_m \left[c_{mk}\cos(\omega_k t) + d_{mk}\sin(\omega_k t)\right]\sin(m\pi\eta). \tag{34}$$

Only $n = m$ terms contribute to the integral over η because of the orthogonality of the sin function. Likewise, only $j = k$ terms contribute to the time average of *Nu*. Thus, the time average net transport is given by

$$\langle Nu\rangle = Pr^2\sum_j \hat{G}r_j^2 \sum_n \frac{1}{\left(n^4\pi^4 + \Omega_j^2\right)\left(n^4\pi^4 + \Omega_j^2 Pr^2\right)} \tag{35}$$

which for $\Omega \gg 0$ becomes

$$\langle Nu\rangle \approx \frac{Pr^{1/2}(Pr^{3/2} - 1)}{2^{3/2}(Pr^2 - 1)}\sum_j \frac{\hat{G}r_j^2}{\Omega_j^{7/2}} \tag{36}$$

If the $\hat{g}(f)$ is specified in terms of a power spectral density function of frequency, PSD(f), the time average *Nu* can be approximated as

$$\langle Nu\rangle \approx \frac{\beta^2(\Delta T/L)^2 a}{\pi^{7/2}2^5\nu^{1/2}}\frac{Pr^{1/2}(Pr^{3/2} - 1)}{(Pr^2 - 1)}\int \frac{\mathrm{PSD}(f)}{f^{7/2}}\,\mathrm{d}f. \tag{37}$$

3.1. Estimated transport resulting from quasi-steady accelerations

An instrumented flow cell in the form of an adiabatic cylinder with differentially heated ends was flown on STS-95 to measure the effects of the residual accelerations [14]. The essential parameters are: $a = 2.54$ cm, $\beta = 0.00025/^\circ$C, $\Delta T/L = 4^\circ$C/cm, $\nu = 0.01$ cm^2/s, and $Pr = 7$. For 1 μg acceleration normal to the thermal axis, $Gr_y = 0.408$, $Ra_y = 2.85$, $u_{max} = 1.03$ microns/s, $\Delta T_{max} = 1.29^\circ$C, $N = 0.00575$. The ΔT_{max} is the temperature difference at the walls in the core region due to the counter flow. The small value for *Nu* indicates the convective transport is negligible for this case. However, the ΔT_{max} predicted from Eq. (19) was close to the observed measurements for estimated accelerations ranging from 0.1 to 1.4 μg [15].

For 1 μg, the effect of stabilizing/destabilizing axial gradients is minimal. However, if the acceleration is increased to 10 μg, the effect can be significant as may be seen in Fig. 2. The dashed line is for adiabatic walls (Eq. (15)) and the solid line is for conducting walls (Eq. (21)). In either case, the $Ra_x = 28.5$ at $\theta = 0$ (destabilizing configuration) is below the critical value for over-turning flow.

4. Effects from single frequency periodic accelerations

4.1. Phase relationships

It is instructive to examine the relative phase relationships between the flow and thermal perturbation as a function of Ω by examining the coefficients of the dominant terms in Eqs. (25) and (26). To simplify matters, we set $g_x = 0$ and consider only the steady state solution. The phase angle between the main part of U and the acceleration is given by $\arctan(A_1/B_1)$ while the phase angle between the major portion of Θ and the acceleration is given by $\arctan(-D_1/-C_1)$.

For $\Omega \ll 1$ (quasi-steady), the flow follows the acceleration and the temperature perturbation is 180° out of phase. For $\omega t = 0$, the acceleration is along the $+y$ axis, the flow is in the $-x$ direction in the lower of the chamber and in the $+x$ direction in the upper half. The result is a warming of the lower half as the flow carries heat from the

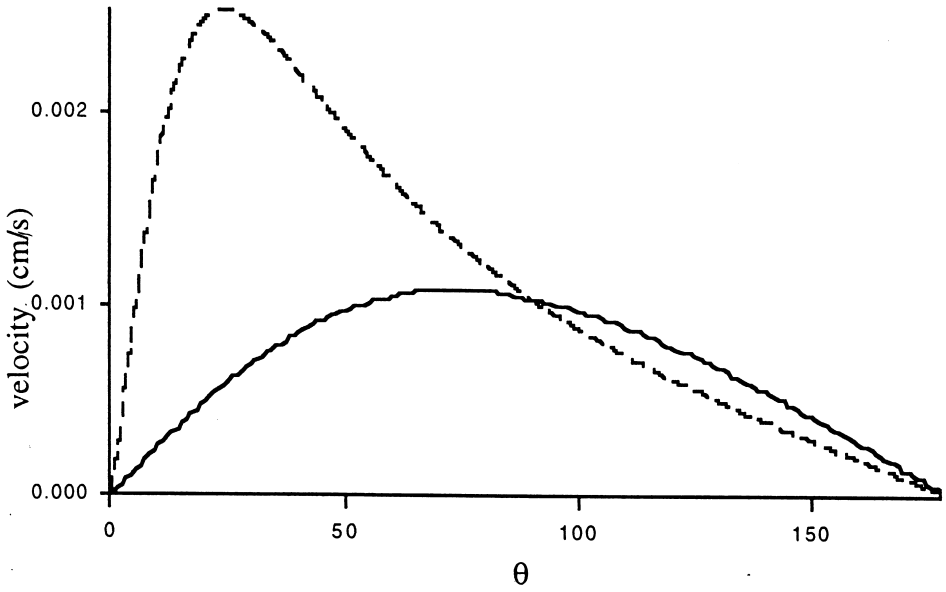

Fig. 2. Maximum core velocity in the flow cell example as a function of the angle the g-vector makes with the thermal gradient. The dashed line corresponds to a chamber with adiabatic walls, the solid to conducting walls. The acceleration is 10 micro-g, which gives a Rayleigh number for this system of 28.5 putting it below the threshold for unstable convection. Thus, the flow goes to zero at $\theta = 0$ since there is no acceleration component normal to a density gradient.

source to the sink, and opposite in the upper half. There is a significant difference between the temperature perturbation caused by the adiabatic versus conducting wall boundary condition because the normal isotherm for the adiabatic condition is advanced by the flow while the isotherm remains pinned to the wall in the conducting case. The $-U\Theta$ product is doubly periodic and is maximized because the U and Θ are 180° out of phase. This situation persists through $\Omega = 1$, but around $\Omega = 10$, the phase relations begin to change rapidly.

When $\Omega = \pi^2$, the phase angle between U and the acceleration becomes 45° and rapidly approaches 90° as Ω increases, which is consistent with the findings of Thevenard [4]. The coefficient C_1 changes sign when $\Omega^2 Pr > \pi^4$ and the phase angle between the acceleration and Θ rapidly approaches 360° as Ω increases. The phase relations between U and Θ are illustrated in Figs. 3 and 4. Also, as may be seen in Fig. 4, the isotherms for adiabatic wall conditions become virtually indistinguishable from the conductive wall conditions as Ω increases past 100 because the flow does not persist long enough to move the isotherm much beyond its average position. This is important because in most applications of interest, Ω will be large enough so that the closed form solutions for the Nusselt and Sherwood numbers will apply regardless of the assumptions made about the heat and mass transfer to the walls.

4.2. Effect of a stabilizing gradient on periodic accelerations

The system described in Example 1 with conductive walls is used as an example to illustrate the effect of a stabilizing gradient on transport. For various values of g_x, g_y, and f, Table 1 gives the resulting Ω, $\hat{N}u$ and $\langle Nu \rangle$. Note that a 1 g stabilizing gradient has a significant damping effect on very low frequency oscillations, but this damping diminishes rapidly as frequency is increased. This suggests that it may be possible to study the effects of g-jitter encountered in spacecraft on Earth by applying horizontal oscillations to a flow cell or a solidification experiment in a thermally stable configuration (hot over cold). (Actually, this possibility was first suggested by Zavarykin et al. [16].)

4.3. Effect of start-up transients

Eqs. (25) and (26) contain the effects of the start-up transients for $g(t) = \hat{g}\cos(\omega t)$. Assuming both U and Θ are 0 when $t = 0$. For large Ω and small n, the B_n terms in Eq. (25) will dominate; hence, the velocity will oscillate about the origin, $\sim 90°$ out of phase with the acceleration. On the other hand, the center of oscillation for Θ will initially be displaced by C_n. However, since C_n is almost cancelled by $A_n/n^2\pi^2(1 + Pr)$, the transient will die out with a time constant given by

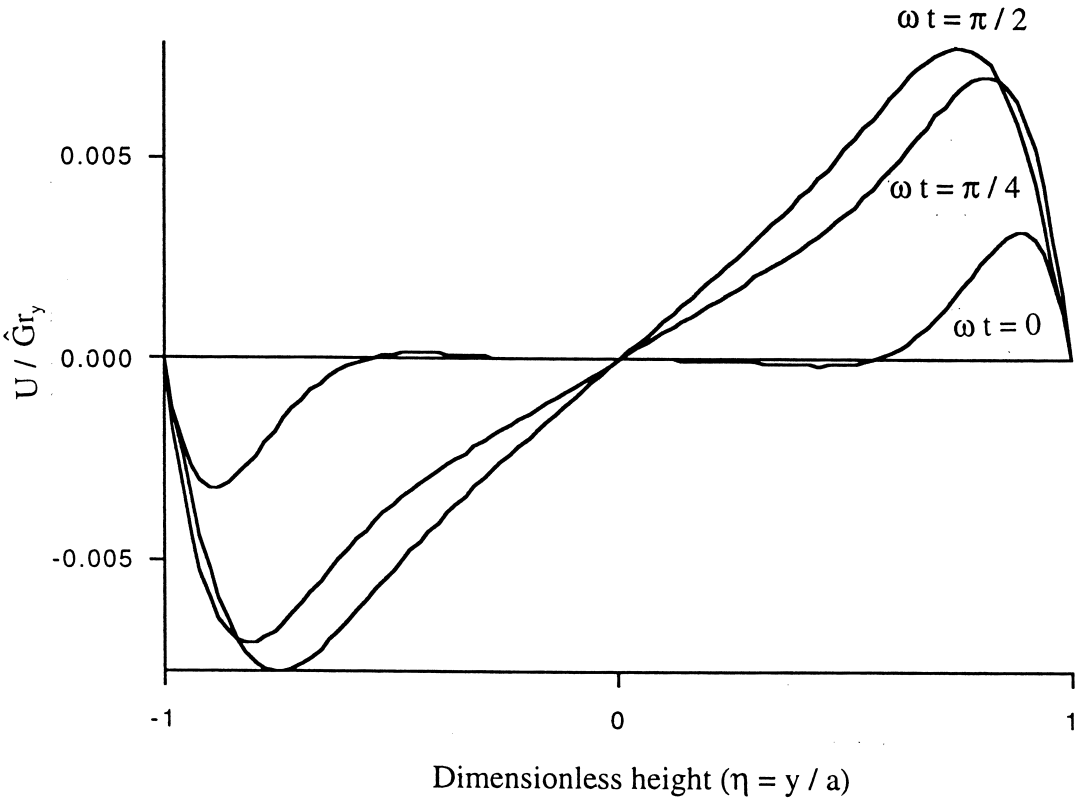

Fig. 3. Evolution of the flow field across the chamber for $\Omega = 100$. The flow field U has been normalized by $\hat{G}r_y$. The phase angle of U relative to the acceleration approaches 90° as Ω get larger and the higher order terms in the series push the peaks closer to the walls.

τ/π^2. The effect on transport will be a small initial increase above the steady state value that damps out exponentially with a time constant of τ/π^2 as shown in Fig. 5(a).

The situation will be dramatically different if the acceleration is given by $g(t) = \hat{g}\sin(\omega t)$. The form of Eqs. (25) and (26) still holds, except in this case the definitions of A_n and B_n as well as C_n and D_n are interchanged. Now the velocity oscillation is initially displaced by its amplitude A_n, which means it doesn't change sign at the beginning. It approaches its steady state behavior with a time constant given

Table 1
Effect of stabilizing gradient on transport from periodic accelerations

g_x/g_0	g_y/g_0	f (Hz)	Ω	$\hat{N}u$	$\langle Nu\rangle$
0	10^{-5}	0	0	0	0.173
0	10^{-3}	0.01	40.5	1.40	0.103
−1	10^{-3}	0.01	40.5	4.37×10^{-5}	1.04×10^{-5}
0	10^{-2}	0.1	405	0.243	3.98×10^{-3}
−1	10^{-2}	0.1	405	0.114	1.9×10^{-3}
0	10^{-2}	1.0	4054	2.76×10^{-4}	1.31×10^{-6}
−1	10^{-2}	1.0	4054	2.90×10^{-4}	1.34×10^{-6}
0	10^{-2}	10	40540	2.87×10^{-7}	4.00×10^{-10}
−1	10^{-2}	10	40540	2.87×10^{-7}	4.00×10^{-10}

by τ/π^2. During this time, the center of oscillation of the temperature perturbation, which goes as the integral of the velocity term, continues to increase. Since now $A_n \sim \Omega^3 Pr^2$ while $C_n \sim \Omega(1+Pr)$, the perturbation dies as $\tau Pr/\pi^2$. The result is an enormous initial increase in transport, as may be seen by comparing Fig. 5(a) and (b).

This increased transport is highlighted in Fig. 6, which is a semi-log plot of the average $\hat{N}u$ for the two cases. Starting with a sine function of acceleration causes an almost three order of magnitude increase in initial transport than if the acceleration had been started with a cosine function. Even though the temperature perturbation persists with a time constant given by $\tau Pr/\pi^2$, the $\hat{N}u$ dies out as τ/π^2 since it is a product of U and Θ. However, if there are other flows, such as a crystallization flow, the transport of heat and/or solute will continue as long as the perturbation in the thermal or solute field persists. This effect was seen by Alexander et al. [3] in the form of a persistent radial segregation after an acceleration was applied in the form of sin ωt.

4.4. Transport from periodic accelerations

Fig. 7 compares the effects of periodic accelerations with those of quasi-steady acceleration as a function of dimensionless frequency. The Nusselt number (or Sherwood number) is normalized by the square of the appropriate Rayleigh number. Since for a typical experiment Ω will be on the order of 100–1000 times the frequency in Hertz, it may be seen that the net transport from the first order flows resulting from transverse periodic accelerations will be negligible compared to the quasi-steady transport for virtually all cases of interest, even though the amplitudes of the periodic components acceleration may be several orders of magnitude higher than the quasi-steady level. Even though the $\hat{G}r_y Pr$ for the periodic accelerations may exceed the range of validity determined for steady accelerations, the model should still be valid since the flow velocity will be limited by the frequency to values that are comparable to the quasi-steady case.

Second order streaming flows may arise from periodic accelerations through the non-linear terms that

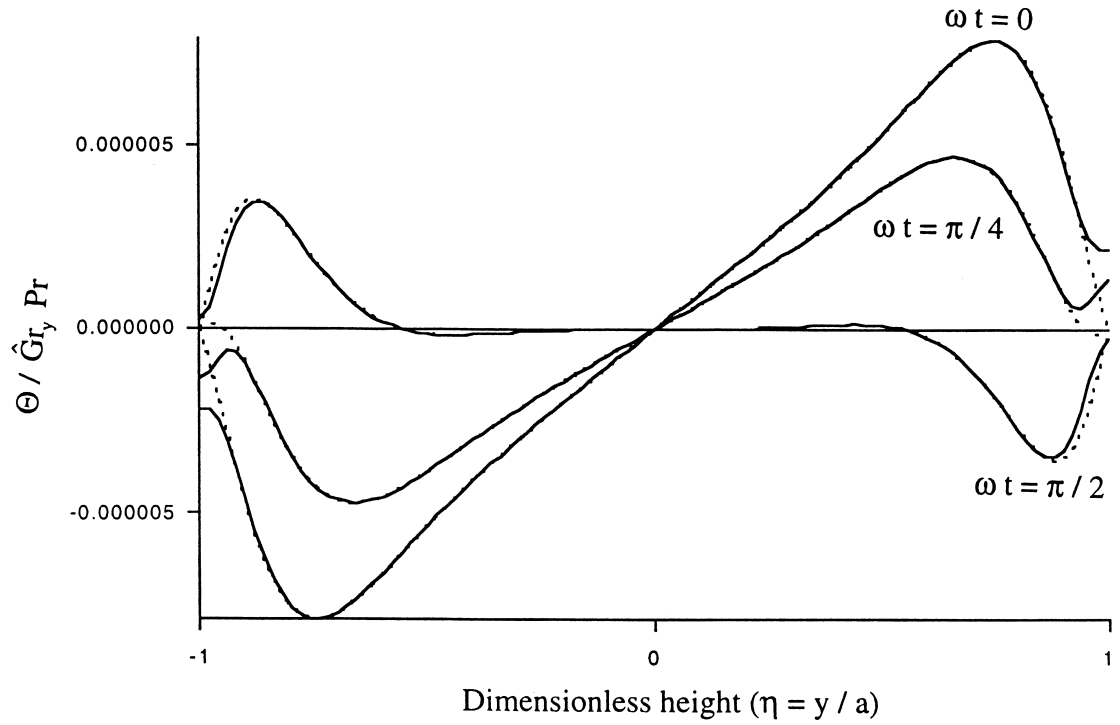

Fig. 4. Evolution of the temperature perturbation with time across the width of the chamber for $\Omega = 100$ and $Pr = 10$. The value of Θ has been normalized by $\hat{G}r_y Pr$. The solid lines represent the case for adiabatic wall boundary conditions and the dotted lines represent the case for conductive walls. As Ω increases, the phase angle approaches 360° relative to the acceleration and the higher order terms in the series push the peak closer to the walls. Also as Ω increases, the isotherms for the adiabatic boundary condition are not able to move very far from their neutral point; thus they become virtually indistinguishable from conductive wall isotherms.

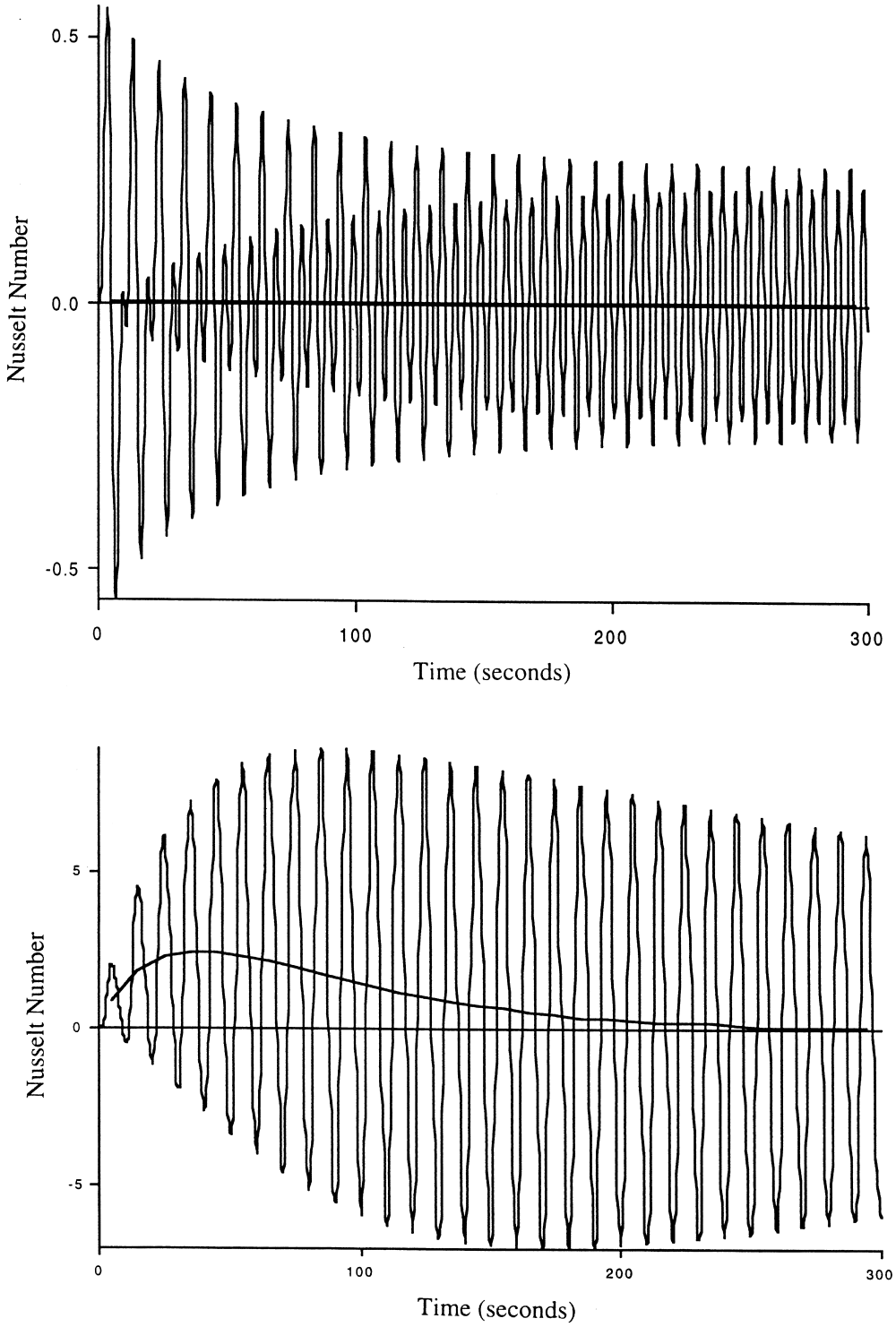

Fig. 5. Nusselt number computed for the flow cell example as a function of time during the start-up transient. The periodic acceleration has an amplitude of 10 mg and a frequency of 1 Hz. (a) For $g(t) = \hat{g}\cos(\omega t)$ the time average Nusselt number rises to a peak of 0.0067 in about 15 s. (b) For $g(t) = \hat{g}\sin(\omega t)$ the time average Nusselt number rises to a peak of 2.46 in about the same time.

dropped out of the model in the limit of vanishingly small aspect ratios. Although such flows are of second order, they could produce significant transport because of their non-zero time average. These flows have been treated extensively in the literature [1,5,6], but no predictive theory for the transport resulting from such flows has been developed. Gershuni ([6], Chapter 3.1) computed these secondary flows in a square chamber with conductive walls and finds that they form four symmetrical counter rotating vortices with zero net stream function for vibrational Rayleigh numbers less than 15000. At this point, a bifurcation occurs in which two of the cells merge to form an asymmetrical flow pattern with a non-zero stream function. The Nusselt number increases linearly with increasing vibrational Rayleigh number until the bifurcation point is reached, after which it increases somewhat because of the increased transport from the asymmetrical flow field. This behavior was found to be insensitive to the Prandtl number for $Pr > 1$. Gershuni's definition of vibrational Rayleigh number is equivalent to $8\hat{G}r_y^2 Pr/\Omega^2$ in the present notation. The Nusselt number for the second order nonlinear flows from his result may be expressed as $Nu^* = \hat{G}r_y^2 Pr/9375\Omega^2$ for $\hat{G}r_y^2 Pr < 1875\Omega^2$. The transport from these nonlinear effects is also shown in Fig. 7. Gershuni also finds that the Nu increases for $A > 1$ (cases for $A < 1$ were not reported), but since the nonlinear terms vanish in the limit of $A \to 0$, it seems reasonable to consider the $A = 1$ case as a upper limit for $A < 1$. The transport from these second order flows becomes more important than the first order effects at the higher frequencies and larger Pr (or Sc). Even so, it still appears that the quasi-steady accelerations will provide the primary transport in most microgravity experiments of the type considered in this analysis.

Non-zero time average flows may also develop if a periodic acceleration has both axial and transverse

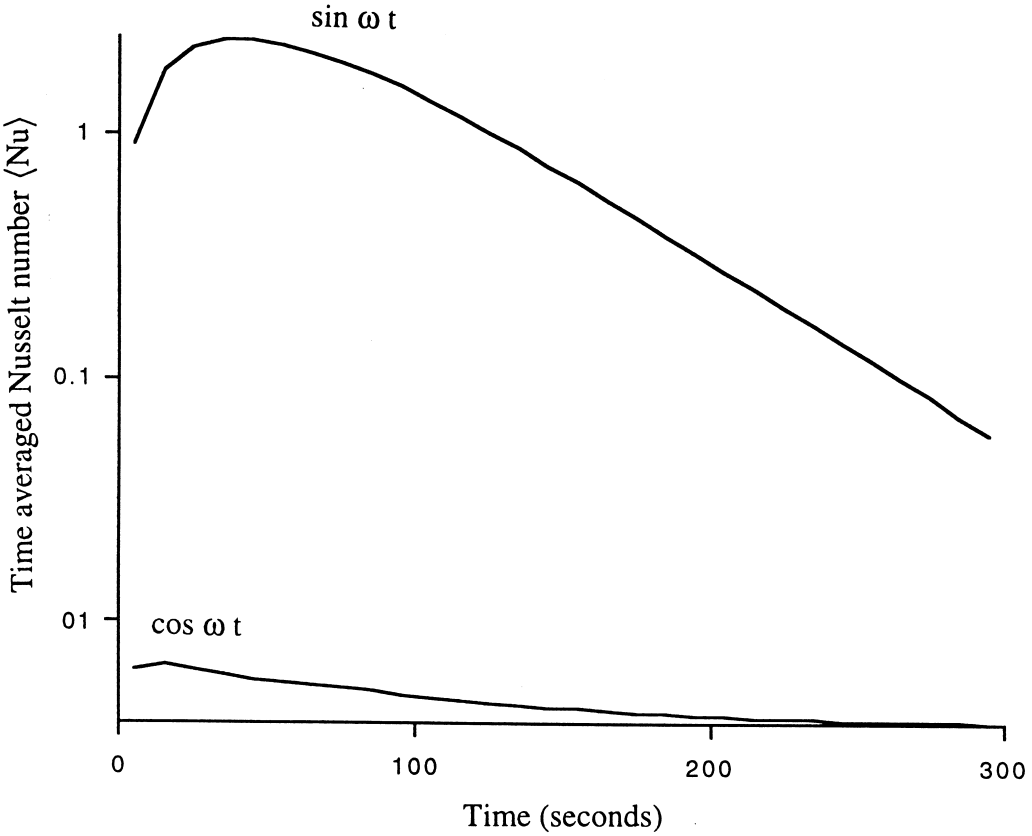

Fig. 6. Semi log plot of the time averaged Nusselt number from Fig. 5. The upper curve is for the sin ωt case and the lower curve is the cos ωt case. Note that the magnitude of the transport during the start-up transient for the sin ωt case is almost three orders of magnitude greater than the final steady state value; whereas the transport during the start-up transient for the cos ωt is only fractionally higher than the steady state value. In both cases the time average Nusselt number falls to the steady state value of 0.0038 with a relaxation time given by τ/π^2 or 65 s.

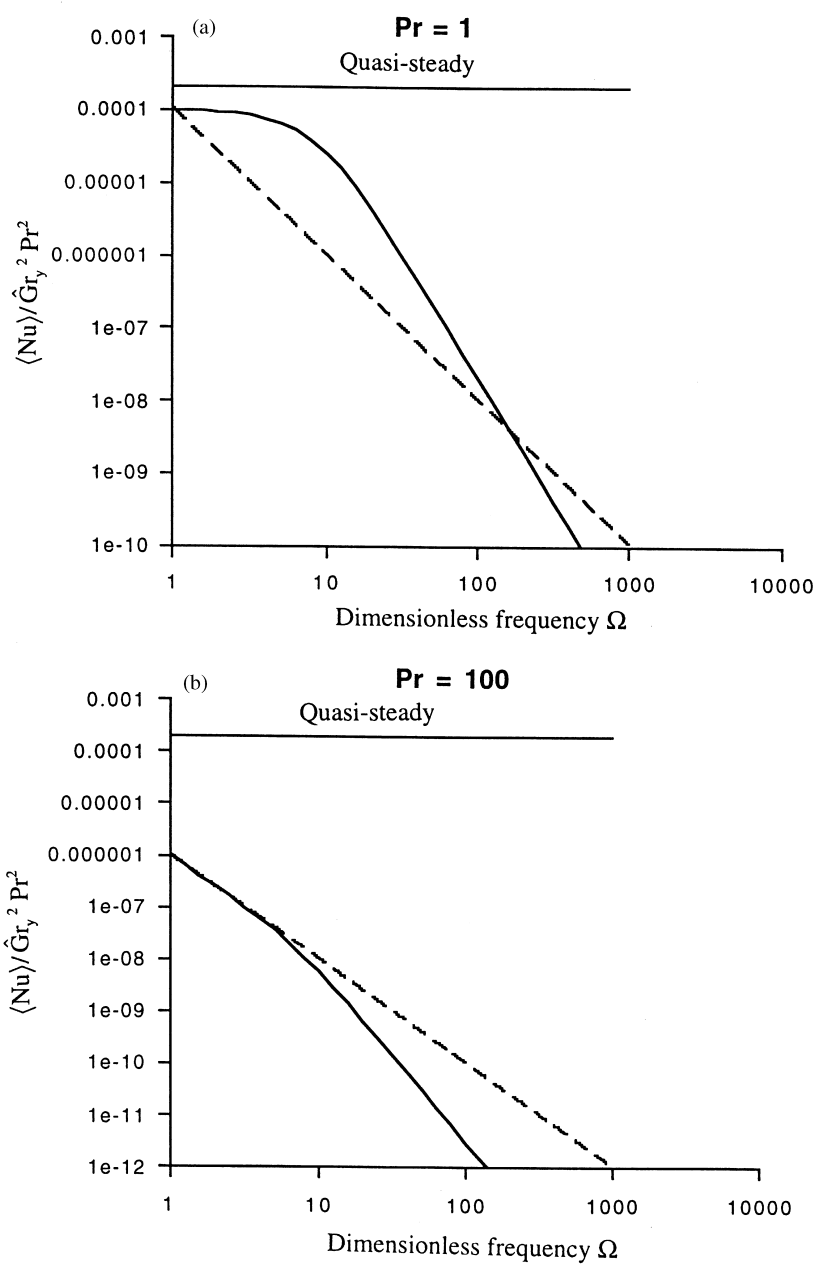

Fig. 7. Comparison of the transport (Nusselt number divided by the square of the Rayleigh number) from quasi-steady acceleration, time averaged transverse first order periodic acceleration (solid curve) and the second order streaming flows from the nonlinear terms in the momentum equation (dashed lines). (a) For $Pr = 1$ and (b) for $Pr = 100$. The dashed curves are taken as upper limits since they were computed for a square chamber and the nonlinear terms must vanish in the limit of 0 aspect ratio. At the higher frequencies and higher Prandtl numbers, the second order terms become more important than the first order flows because they produce non-zero time average flows. However, for most systems of interest, the quasi-steady accelerations will be the most important.

components [17]. This comes about because during half of a cycle, the axial flow encounters a destabilizing gradient, which increases the flow, then during the second half of the cycle, it encounters a stabilizing gradient which decreases the flow. The result is an oscillating flow similar to the flows described in the present model, except there will be a non-zero time average. A crude analysis of the transport from this type of flow suggests that the Sherwood number scales as $\hat{G}r^4Sc^2\sin^2\theta\cos^2\theta\Omega^{-4}$ [18]. A more refined analysis based on the model presented in this work is being developed.

5. Effect of multiple frequency disturbances

A typical integrated PSD for a Shuttle mission is on the order of 10^5 $(\mu g)^2$, which corresponds to an RMS of ~ 300 μg. The Shuttle has structural modes around 3–7 Hz; however, a significant contribution to the integrated PSD comes from the 17 Hz dither frequency of the KU band antenna and its harmonics. The integral of the PSD weighted by the inverse 7/2 power of frequency yields ~ 10 $(\mu g)^2$ $s^{7/2}$. Factoring out $\hat{G}r$ (1 μg) from the numerator of the sum in Eq. (36) and Ω (1 Hz) from the denominator of the sum, Eq. (36) becomes equivalent to Eq. (31) with $g = 10^{1/2}$ μg and Ω computed for $f = 1$ Hz. If one take a conservative estimate that $\Omega = 100f$, the ratio of $\langle Nu\rangle$ from the integrated effect of the g-jitter spectrum to the quasi-steady Nu for 1 μg is $0.00167/Pr^2$. Again it is seen that the transport will be dominated by the quasi-steady acceleration. (The multi-frequencies from the nonlinear effects are not additive, hence their combined effects must be computed numerically.)

6. Conclusions

A simple analytical model has been developed that describes the heat and mass transport in a low aspect ratio (length $\gg$ width) chamber for steady and periodic acceleration. For steady accelerations normal to the density gradient, the Nusselt number (ratio of convective to diffusive thermal transport) and the Sherwood number (ratio of convective to diffusive solutal transport) scale as $(GrPr)^2$ and $(GrSc)^2$, respectively. The predictions using this simple analytical model appear to be qualitatively consistent with observed effects of quasi-steady acceleration in the instrumented flow cell flown on STS-95.

Singularities are present in the quasi-steady model when the axial Rayleigh numbers reaches certain positive critical values that depend on the thermal boundary values. These singularities correspond to the thresholds for unstable Rayleigh Benard-type convection as shown by comparison with linear stability analysis. Periodic flows, excited by transverse vibrations, tend to stabilize these flows. The singularities vanish in the presence of periodic transverse accelerations, but the resulting flows can still get large at very low frequencies.

Periodic oscillations normal to the density gradient are seen in the first order theory to be an ineffective mechanism for heat and mass transport in a low aspect ration chamber. The velocity and temperature perturbation become almost 90° out of phase with one another as frequency increases. Net heat and mass transport are predicted to fall off as the inverse 7/2 power of frequency. Only the very lowest frequencies (less than 1 Hz) could be expected to produce significant effects and then only for acceleration amplitudes considerably larger than would be expected in normal Space Shuttle operations. Although the quasi-steady thermal transport is significantly affected by whether the walls are conductive or insulated, this distinction vanishes at higher frequencies, thus allowing the simpler formulation for conductive walls to be used for both thermal and solutal transport.

It was shown that a large stabilizing axial gradient will significantly damp very low frequency (sub hertz) transport, but this damping effect diminishes as frequency is increased. This suggests the possibly of being able to test the high frequency predictions of the model on the ground by applying horizontal periodic accelerations to a test cell or solidification experiment with a vertical stabilizing thermal gradient (hot over cold).

The effects of start-up transients are highly dependent on the phase of the acceleration at $t = 0$; i.e., whether the acceleration is represented as a sine or cosine function. There is virtually no additional transport if the acceleration is represented by a cosine function, but if the acceleration is represented by a sine function, there will be an initial non-zero average velocity, which can produce a very large temperature or solute excursion. The resulting transport can be orders of magnitude larger than the steady state value. The persistence of the temperature or concentration perturbation is proportional to the Prandtl or Schmidt numbers, respectably, which can be quite long. However, the net transport dies with the decay time of the flow velocity. (However, if there is additional steady state flow such as the growth velocity in a solidification experiment, the transport will continue as long as the perturbation persists, as was seen by Alexander [3].)

Since the nonlinear terms in the momentum equation vanish in the limit of small aspect ratio, the effects of multiple frequencies should be additive. This allows the total transport to be expressed in terms of the integral of the power spectral density of the accel-

eration weighted by the inverse 7/2 power of frequency. Using typical power spectral densities observed during Shuttle operations, the transport from periodic accelerations in typical experiments to which this model is applicable should be virtually undetectable. In any case, it would appear that the effects of quasi-steady accelerations would overwhelm any periodic acceleration that could be reasonably expected, even though the latter may have much higher amplitudes.

The role of the start-up transients in producing net transport also needs to be better understood. As was shown, whether the acceleration is applied as a sine or cosine function can make orders of magnitude difference in the initial transport. Whether such effects play a significant role in the effective mass transfer in space experiments is not clear.

More work is required in order to understand the effects of g-jitter on space experiments. The most critical need is detailed experimental time-resolved flow data measured in a well-defined system in which controlled single and multiple frequency accelerations can be applied. Such data would serve to test and refine the various analytical and computational models that have been proposed and could lead to a more general understanding of this important and perplexing problem.

References

[1] Y. Kamotani, A. Prasad, S. Ostrach, Thermal convection in an enclosure due to vibrations aboard a spacecraft, AIAA Journal 19 (1981) 511–516.

[2] J.I.D. Alexander, J. Ouazzani, F. Rosenberger, Analysis of the low gravity tolerance of Bridgman–Stockbarger crystal growth I. Steady and impulse accelerations, Journal of Crystal Growth 97 (1989) 285–302.

[3] J. Alexander, S. Amiroudine, J. Ouazzani, F. Rosenberger, Analysis of the low gravity tolerance of Bridgman–Stockbarger crystal growth II. Transient and periodic accelerations, Journal of Crystal Growth 113 (1991) 21–38.

[4] D. Thevenard, H. Ben Hadid, Low Prandtl number convection in a rectangular cavity with longitudinal thermal gradient and transverse g-jitters, International Journal of Heat and Mass Transfer 34 (1991) 2167–2173.

[5] S. Monti, R. Savino, Microgravity experiment acceleration tolerability on space orbiting laboratories, Journal of Spacecraft and Rockets 33 (1996) 707–716.

[6] G.Z. Gershuni, D.V. Lyubimov, Thermal Vibration Convection, Wiley, West Sussex, England, 1998.

[7] P.S. Perera, Liquid diffusion couple in a microgravity environment, Thesis, Department of Mathematical Sciences, Carnegie Mellon University, Pittsburgh, PA, 1997.

[8] D. Cormack, L. Leal, J. Imberger, Natural convection in a shallow cavity with differentially heated end walls, part I. Asymptotic theory, Journal of Fluid Mechanics 65 (1974) 209–229.

[9] D. Cormack, L. Leal, J. Seinfeld, Natural convection in a shallow cavity with differentially heated end walls, part II. Numerical solutions, Journal of Fluid Mechanics 65 (1974) 231–246.

[10] J. Imberger, Natural convection in a shallow cavity with differentially heated end walls, part III. Experimental results, Journal of Fluid Mechanics 65 (1974) 247–260.

[11] A.E. Gill, The boundary-layer regime for convection in a rectangular cavity, Journal of Fluid Mechanics 26 (1966) 515–536.

[12] R.J. Naumann, Stabilizing/destabilizing effects of axial accelerations in Bridgman growth, Journal of Crystal Growth 165 (1996) 129–136.

[13] A. Bejan, C. Tien, Fully developed natural convection in a long horizontal pipe with different end temperatures, International Journal of Heat and Mass Transfer 21 (1978) 701–708.

[14] R.J. Naumann, G. Haulenbeek, Japanese–US Thermal Science Accelerometer Project (JUSTSAP), STAIF Conference, Albuquerque, NM, 1999. Proceedings to be published by the American Institute of Physics, New York.

[15] R.J. Naumann, G. Haulenbeek, High precision flow cell accelerometer for measuring quasi-steady microgravity accelerations, in: 18th International Microgravity Measurements Group Meeting, Cocoa Beach, FL, NASA Glen Research Center, Cleveland, OH, 1999, pp. 181–195.

[16] M.P. Zavarykin, S.V. Zorin, G.F. Putin, Experimental study of vibrational convection, Fluid Mechanics 37 (1985) 267–268 (translation of Soviet Physics Doklady).

[17] J.I.D. Alexander, Residual gravity jitter effects on fluid process, Microgravity Science and Technology VII/2 (1994) 131–136.

[18] R.J. Naumann, Effects of transient and periodic accelerations on heat and mass transport, in: C. Lundquist, F.C. Wessling, L.D. Jones (Eds.), Materials Development in Space, CMDS Final Report, University of Alabama at Birmingham Press, Birmingham, AL, 1997, pp. A1–A37.